Proceedings of IMECE2005
2005 ASME International Mechanical Engineering Congress and Exposition
November 5-11, 2005, Orlando, Florida USA

IMECE2005-82012

NIST DEVELOPMENT OF REFERENCE MATERIAL SCAFFOLDS FOR TISSUE ENGINEERING*

Joy P. Dunkers
Polymers Division
National Institute of Standards and Technology, Gaithersburg, MD

Stefan D. Leigh
Statistical Engineering Division
National Institute of Standards and Technology, Gaithersburg, MD

Marcus T. Cicerone
Polymers Division
National Institute of Standards and Technology, Gaithersburg, MD

Forrest A. Landis
Polymers Division
National Institute of Standards and Technology, Gaithersburg, MD

Francis W. Wang
Polymers Division
National Institute of Standards and Technology, Gaithersburg, MD

John A. Tesk
Polymers Division
National Institute of Standards and Technology, Gaithersburg, MD

ABSTRACT

In consultation with ASTM and other stakeholders in Tissue-Engineered Medical Products (TEMPs) industry, the National Institute of Standards and Technology (NIST) initiated a project designed to produce Reference Material scaffolds for tissue engineering. The rationale for Reference Material scaffolds was developed through several NIST/Industry workshops. In brief, Reference Material scaffolds have multiple uses: facilitating the development and the validation of new test methods that measure interactions among various components of a TEMP; comparison with other scaffolds and scaffold materials in terms of cellular responses, biodegradation, and releases of growth factors; and comparisons of responses among various cell lines. The primary customers for Reference Material scaffolds are expected to be the TEMPs industry, academic researchers, regulators, and standards developing organizations. There are many properties of a TEMP that warrant development of multiple Reference Material scaffolds. Currently, NIST is defining a set of Reference Material scaffolds based on geometric descriptors such as permeability, pore volume, pore size distribution, interconnectivity, and tortuosity. In consultation with ASTM, NIST is testing three candidate scaffolds produced by: three dimensional (3-D) printing, stereolithography, and fused deposition modeling (FDM). Scaffolds made by these methods have been obtained from Mayo Clinic (Rochester, MN), Case Western Reserve University (CWRU) (Cleveland, OH), and Osteopore International (Singapore), respectively, for structural characterization. These prototype scaffolds, with well-defined architectures, have been selected to address the following items of interest: 1) establishment of useful functional definitions of porosity content, interconnectivity, and pores; 2) evaluation of testing methods listed in the *Standard Guide for the Porosity of Polymeric Scaffolds for Use in Tissue-Engineered Medical Products*, which is being drafted by ASTM. Currently, NIST and the Center for Devices and Radiological Health of the Food and Drug Administration, as well as other groups from US and foreign laboratories, are actively carrying out cross-validation test of these prototype scaffolds.

INTRODUCTION

The field of tissue engineering involves "the application of the principles and methods of engineering and life sciences towards the fundamental understanding of structure-function relationships in normal and pathological mammalian tissues and the development of biological substitutes that restore, maintain or improve tissue function" (1). A major effort of tissue engineering aims at growing the pertinent cells *in vitro* or *in vivo* into a 3-D body of tissue that fits the wound site. This aim is often achieved by seeding cells into porous matrices, referred to as scaffolds, and cultivating the cells to grow and organize for tissue function. Alternatively, cells will migrate into scaffolds when activated with chemotactic or haptotactic molecules from the surrounding healthy tissues or model tissues.

Sachlos and Czernuszka (2) have reviewed the limitations of current tissue engineering scaffolds made from biodegradable synthetic or natural polymers by conventional

fabrication methods. This includes materials made by solvent-casting particulate-leaching, gas foaming, fiber meshes/fiber bonding, phase separation, melt molding, emulsion freeze drying, solution casting, and other techniques. Among the limitations identified are: 1) inadequate control of pore size, pore geometry, spatial distribution of pores and construction of internal channels within the scaffolds and 2) diffusion constraints due to the foam-like structures that prevent the cells from migrating deep into the scaffolds. This results in a decrease in cell viability and eventually cell death due to a lack of nutrients and oxygen and insufficient removal of waste products. To increase the mass transport of oxygen and nutrients, solid freeform fabrication (SFF) technologies can be used for scaffold production. With SFF technologies, layered manufacturing strategies are used to produce scaffolds with customized external shape and predefined and reproducible morphology.

In view of the need to control of topographical and morphological parameters of a scaffold, the characterization of scaffold morphology was considered an important focus area by the participants at a Workshop on Reference Data for the Properties of Biomaterials held at the NIST on July 27, 2000. The participants identified the Reference Materials most needed for tissue engineering as three-dimensional scaffolds of known porosity, interconnectivity, surface and bulk chemistry, physical and mechanical properties, and cellular activity (3).

In addition, ASTM, through its F04.42 Subcommittee on Biomaterials and Biomolecules for TEMPs, also recognized this need. The subcommittee drafted a *Standard Guide for Assessing the Porosity of Polymeric Scaffolds for Use in Tissue-Engineered Medical Products*. On November 19, 2003, the subcommittee established an ASTM Task Force (F04.42.06) for the development of reference scaffolds for TEMPs.

In collaboration with ASTM Task Force F04.42.06, NIST sent in November 2004 three types of prototype scaffolds to US and foreign laboratories for inter-laboratory characterization of porosity. The results from this characterization effort will be used by NIST in the development of NIST Reference Material scaffolds for use for the TEMPs industry and other standards developing organizations. In this paper, the results of the characterization work that was carried out at NIST are presented.

The goal of this work was to establish a multi-step methodology to evaluate the quality of candidate reference scaffolds in a quantitative manner. (4) In this context, the term "quality" refers to an evaluation of the microstructure descriptors of total pore volume, pore volume distribution, and pore length distribution (or strut gap). These descriptors are specific to this analysis and represent a contribution to consensus definitions on scaffold structure.

The first step of the methodology was to generate a model scaffold based on expected geometry for all three scaffold types. Second, the descriptors of total pore volume, pore volume distribution, and pore length were extracted from 3-D X-ray micro-computed tomography (μ-CT) image sets of the models and manufactured scaffolds. Last, statistics were generated on the descriptors so that two questions could be answered: 1. How accurately did the fabricated scaffolds replicate the model? 2. How uniform in structure were the fabricated scaffolds?

EXPERIMENTAL[#]

Three types of scaffolds were defined for morphological studies: 1) scaffolds made at Case Western Reserve University (CWRU scaffolds), 2) scaffolds made at Mayo Clinic College of Medicine (Mayo scaffolds), and 3) scaffolds made at Osteopore International, Singapore (Osteopore scaffolds). CWRU scaffolds were made by 3D Systems (Valencia, CA) from Accura si 10 resin using stereolithography. The CWRU manufactured scaffolds are designated as Part #2, Part #4, and Part #17. The fabrication of Mayo scaffolds entailed: 1) making the negative molds of the scaffolds with the use of a 3-D printing process, 2) filling the molds with poly(propylene fumarate) macro-monomer, together with 1-vinyl-2-pyrrolidinone, which crosslinked the macro-monomer by free radical polymerization in the presence of benzoyl peroxide and dimethyltoluidine, and 3) dissolving the molds with an appropriate solvent, e.g., methylene chloride. The Mayo manufactured scaffolds were designated as Part #3 and Part #4. Both Mayo scaffolds and CWRU scaffolds were designed to have the exterior dimensions of (7.1 mm x 7.1 mm x 7.1 mm), cubic pores with 0.6 mm on a side, and struts with a cross section of 0.5 mm x 0.5 mm. Osteopore scaffolds were made from poly(caprolactone) by fused deposition modeling with $0^o/60^o/120^o$ lay-down pattern. Each layer of the scaffolds was designed to be made of cylindrical struts 0.4 mm in diameter, with a strut gap of 1.0 mm separating adjacent struts. The Osteopore manufactured scaffolds are designated as Part #1, Part #2, and Part #3.

μ-CT was performed for morphological analysis. The μ-CT images were generated by a Skyscan 1072 micro-computed tomography (μ-CT) scanner. The data set was output as individual, 2D bitmap files. In this work, the error is a type B standard uncertainty from the resolution limit of each image set. The error is expressed as a relative uncertainty for the total pore volume and as a standard deviation for the variational distance. The standard deviations for the mean pore volume and pore length (strut gap) are intended to show the distribution of values for the parts as compared to the theoretical (model) values. The uniformity of parts among a scaffold type is expressed by X^2.

For computational analysis, a 3-dimensional image analysis package called Blob3D was used to extract pore size distribution and pore volume distribution for the model scaffolds and for the μ-CT images for all parts for the three scaffold types. Blob3D was written by R. Ketcham and his group using Interactive Data Language (IDL, Research System, Inc.). Blob 3D de-noises, thresholds, and segments the pores into unit cells (UCs). Total pore volume was calculated as the summation of the UC pore volumes divided by the total volume of the scaffold. The total volume of the scaffold was calculated using the area of the cropped 2D slices multiplied by the number of slices. From each UC, pore volume distribution (PV) was extracted by summing the volume of all the voxels present in each UC. Then, each unit cell was fitted with an ellipsoid to extract the long and short axis lengths. The long axis was used as the pore length (PL).

Variational distance (VARD) is a measure of the similarity of two distributions. (5) An empirical version of VARD is computed by first generating histograms of the data and model with the same binning schemes. At each bin, the absolute value of the difference between the model and experimental results is

computed. These numbers are summed over all bins and the result is divided by 2. VARD varies from 0 (two identical distributions) to 1 (two mutually exclusive distributions). In this paper, we use empirical VARD as a statistical measure of quality of scaffold as compared to its model. The smaller the number, the closer the experimental pore volume to its model. In addition, PV and PL uniformities were calculated for CWRU and Osteopore scaffolds. A representative computation of pore uniformity is shown in Table 1. The smaller the number, the more similar the scaffolds. The $\pm$ 1 σ uncertainty associated with the variational distance was calculated by bootstrapping. (6)

RESULTS AND DISCUSSION

The methodology for structural quantitation is illustrated below with the CWRU scaffold. Figure 1 shows the CAD-based model for the CWRU and Mayo scaffolds. To further understand the imaging results on the parts, a theoretical analysis was performed on the scaffold using only the design dimensions to extract the quantities of interest. These scaffolds have 216 pores distributed into 4 distinct UCs which are shown in Figure 2. There are 64 UCs (shown in Figure 2A) found in the interior of the scaffold. These UCs have a PV of 0.756 mm^3 and PL of 1.1 mm. Figure 2B displays a UC found on each face of the cube with 1 long axis. There are 94 of these UCs that have a PV of 0.846 mm^3 and a PL of 1.35 mm. The UC in Figure 2C has 2 long axes and a PV of 0.936 mm^3. There are 48 of these UCs in the scaffold with a PL of 1.35 mm. Lastly, there are 8 UCs shown in Figure 2D that are found on each corner of the scaffold. These unit cells have a PV of 1.026 mm^3 and a PL of 1.35 mm. From this analysis, the theoretical total pore volume is 51.1 % by volume.

Figure 3 shows a sub-section of the μ-CT image set from a CWRU scaffold designated as Part 2. The μ-CT reconstruction in Figure 3 and the model scaffold in Figure 1 are qualitatively similar by visual inspection.

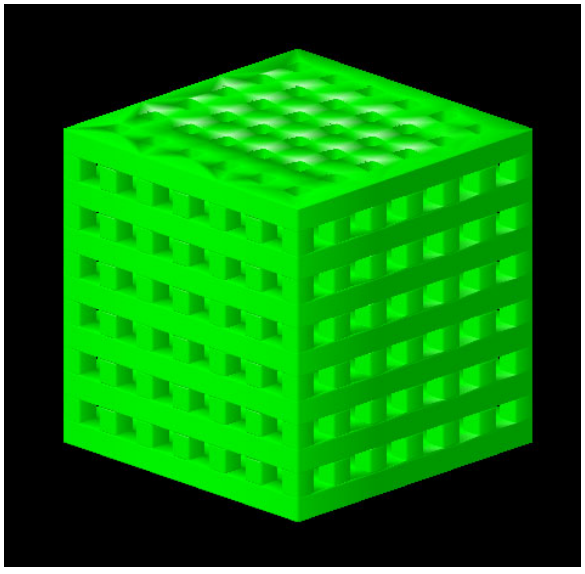

Figure 1: CAD-based model for Mayo scaffolds and for CWRU scaffolds.

Figure 2: Four types of unit cells found in CWRU and Mayo scaffold. A) No long axis, B) 1 long axis, C) 2 long axes, D) 3 long axes.

Figures 4 shows the PV distribution from the μ-CT image (in black) superimposed on the distribution (in red) for the CAD-based model for Part 2. The distribution from the μ-CT image is clearly broader than the distribution from the model. Overall, the distributions exhibit a significant degree of overlap, as shown by relatively low VARDs in Table 1 for the CWRU scaffolds. Table 1 also gives morphological parameters derived from their μ-CT images compared to the parameters derived from the CAD-based model.

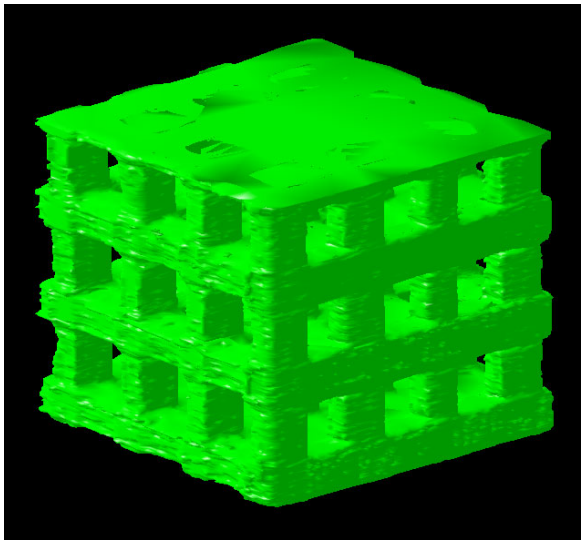

Figure 3: μ-CT image of a sub-section of CWRU scaffold.

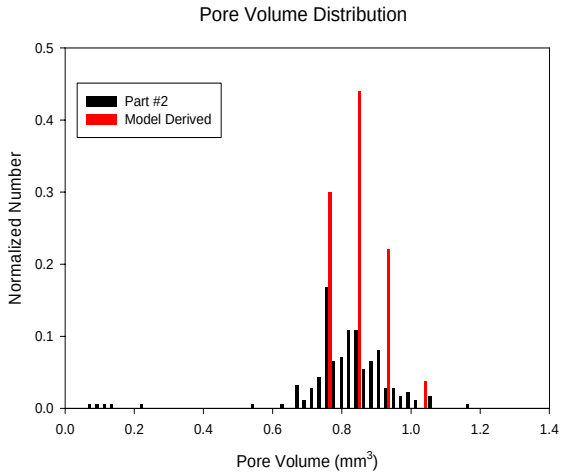

Figure 4: The pore- volume distribution for a CWRU scaffold (Part 2) from the μ-CT image (shown in black), compared with the distribution (shown in red) for the CAD-based model.

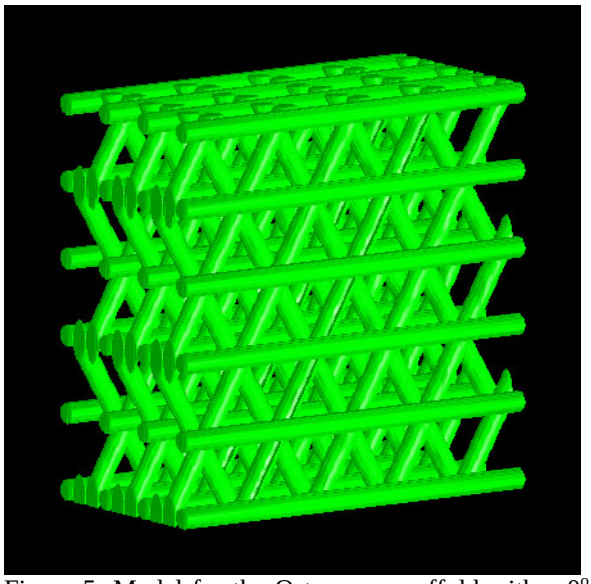

Figure 5: Model for the Osteopore scaffold with a $0^o/60^o/120^o$ lay-down pattern

Similarly, Table 2 gives the morphological parameters for the Mayo scaffolds. It is worth noting that the CWRU scaffolds resembled the CAD-based model much more than the Mayo scaffolds by comparing the values of all the morphological descriptors.

The Osteopore scaffolds had a completely different geometry because of their fabrication design. The model Osteopore scaffold is shown in Figure 5 and contains unit cells having one intrinsic PV and one intrinsic PL. It should be noted that the results from the 3D image quantitation on the model serve as the basis for comparison to the parts rather than purely theoretical values. Table 3 gives the morphological parameters for the Osteopore scaffolds.

CONCLUSIONS

The Mayo scaffolds had VARDs much greater than the CWRU scaffolds. The Osteopore scaffolds also faired worse than the CWRU scaffolds in matching the morphology of the CAD-based model. Further analysis of their uniformity values shows that the large VARDs for the Osteopore scaffolds are not due to structural defects but due to a systematic difference in structure from the model. The Osteopore scaffolds were more uniform in total pore volume than the CWRU scaffolds. Both types of scaffolds had very good uniformity of pore volume and pore length (strut gap). Since the lack of sample-to-sample variation is one of the most important requirements in Reference Materials, the Osteopore and CWRU scaffolds have much merit as Reference Materials. In addition, since Osteopore scaffolds are made of a biodegradable, biocompatible polymer, it is worthwhile to consider them as candidate Reference Materials for the viability of cells in tissue engineering scaffolds. We have initiated work on examining the response of osteoblasts to FDM manufactured scaffolds. (7)

ACKNOWLEDGMENT

We would like to acknowledge Richard Ketcham of the Jackson School of Geosciences, University of Texas at Austin for providing us with Blob3D.

Thanks to David Dean and Malcolm Cooke from CWRU, Michael Yaszemski from Mayo Clinic College of Medicine, and Tan Siow Khoon from Osteopore International for supplying the scaffolds.

REFERENCES

1. R. Shalak and C.F. Fox (1988). Preface. In: *Tissue Engineering*. R. Shalak and C. F. Fox, eds. Alan R. Liss, New York. Pp. 26-29.
2. E. Sachlos and J. T. Czernuszka, European Cells and Materials **5**, 29 (2003).
3. J. A. Tesk, J. Biomed. Mater. Res. (Applied Biomater.) **58**, 463 (2001).
4. J. P. Dunkers, Manuscript in preparation (2005).
5. G. Blom, L. Holst and D. Sandell (1994). *Problems and Snapshots from the World of Probability*, Springer-Verlag.
6. F.B. Efron and R. J. Tibshirani (1993). *An Introduction to the Bootstrap*, Chapman and Hall.
7. T. Dutta Roy, J. J. Stone, E. H. Cho, S. J. Lockett, F. W. Wang, and L. Henderson, Proc. IMECE 2005, Nov. 5-11, Orlando, FL.

DISCLAIMER

#Certain commercial equipment, instruments, or materials are identified here to adequately specify experimental procedure. Such identification is not intended to imply recommendation or endorsement by NIST, nor does it imply that the materials or equipment identified are the best available for the purpose.

Table 1: The morphological parameters, derived from the μ-CT images for the CWRU scaffolds, in comparison with the parameters derived from the CAD-based model.

	Theoretical	Part 2	Part 4	Part 17
Total Pore Volume (%) (relative uncertainty)	51.1	50.0 ± 1.47	50.8 ± 1.47	52.6 ± 1.47
Total Pore Volume Uniformity (mm^3) (X^2)	_____	0.0694		
Mean Pore Volume (mm^3) (± 1 σ)	0.846± 0.074	0.800± 0.143	0.808± 0.159	0.851± 0.115
Pore Volume Uniformity (mm^3) (X^2)		1.83×10^{-4}		
Mean Pore Length (mm) (± 1 σ)	1.28 ± 0.11	1.45± 0.19	1.44 ± 0.23	1.45 ±0.22
Pore Length Uniformity (mm) (X^2)		4.63×10^{-5}		
Variational Distance (volume) (±1 σ)	_____	0.158±0.035	0.087±0.025	0.146+0.031

Table 2: The morphological parameters, derived from the μ-CT images for the Mayo scaffolds, in comparison with the parameters derived from the CAD-based model.

	Theoretical	Part 3	Part 4
Total Pore Volume (%) (relative uncertainty)	51	56.0 ± 1.49	53.0 ± 1.49
Mean Pore Volume (mm^3) (± 1 σ)	0.846 ± 0.074	0.496 ± 0.354	0.218 ±0.316
Mean Pore Length (mm) (± 1 σ)	1.28 ± 0.11	0.98 ± 0.50	0.59 ± 0.58
Variational Distance (volume) (± 1 σ)	_____	0.563 ± 0.018	0.899±0.013

Table 3: The morphological parameters, derived from the μ-CT images for the Osteopore scaffolds, in comparison with the parameters derived from the CAD-based model.

	Model	Part 1	Part 2	Part 3
Total Pore Volume (%) (relative uncertainty)	77.1±2.47	75.6±2.42	75.9±2.43	76.0±2.43
Total Pore Volume Uniformity (%) (X^2)	_____	0.0011		
Mean Pore Volume (mm^3) (± 1 σ)	1.40 ± 0.02	1.01 ± 0.07	1.02 ± 0.06	1.07 ± 0.08
Pore Volume Uniformity (X^2)		2.04×10^{-3}		
Adjusted Variational Distance (volume) (± 1 σ)	_____	0.733±0.085	0.671 ± 0.073	0.730±0.055
Mean Strut Gap (mm) (± 1 σ)	0.98 ± 0.03	1.29 ± 0.09	1.22 ± 0.05	1.30 ± 0.09
Strut Gap Uniformity (mm) (X^2)	_____	2.99×10^{-3}		